Proceedings of the 10th World Congress on Momentum, Heat and Mass Transfer (MHMT 2025)
Barcelona, Spain - April, 2025
Paper No. ENFHT 160
DOI: 10.11159/enfht25.160

Simultaneous Derivation of Temperature and Velocity Fields Using Background-Oriented Schlieren

Zhenggang Ren[1,2], Liang Hu*[1,2], Jing Wang[1,2], Rui Su[1,2], Yingnan Shen[1,2], Xiaodong Ruan[1,2]
[1]State Key Laboratory of Fluid Power and Mechatronic Systems
[2]Engineering Research Center of DLIS, Ministry of Education
Zhejiang University, Hangzhou 310027, China
zhenggang.r@zju.edu.cn; cmeehuli@zju.edu.cn; jing.wang@zju.edu.cn;
srhello@zju.edu.cn; shenyingnan@zju.edu.cn; xdruan@zju.edu.cn;

Abstract **-** This paper presents a cost-effective method to reconstruct velocity distributions using data from the Background-Oriented Schlieren (BOS) technique. The proposed method reconstructs the velocity field by solving the Navier-Stokes (N-S) equations, incorporating the measured temperature difference as an additional force term. This approach reduces the need for predefined boundary conditions and enhances the convergence speed of numerical calculations. Two benchmark cases are presented to demonstrate the effectiveness of the reconstruction method. The first case focuses on reconstructing the velocity field in natural convection within a cubic enclosure, where buoyancy forces dominate the flow. The second case reconstructs the velocity field in mixed convection, where shear stress competes with buoyancy forces. These validation cases confirm that the reconstruction method is applicable in both coupled temperature and velocity flows, as well as in decoupled situations. Both comparisons have been numerically validated by comparing the velocity profile against simulation data, achieving good agreement and demonstrating a maximum error of 1%.

Keywords**:** Natural convection, Mixed convection, Background-oriented schlieren, Velocity reconstruction, Data assimilation

1. Introduction

The immersion technique encompasses various technologies, such as immersion cooling [1], immersion lithography [2] and liquid lens [3], which have elevated the importance of precise control over immersion flow characteristics. Excessive heat dissipation increases the cooling requirements of data centres, while the continuous miniaturization of semiconductor critical dimensions (CD) demands mK-level temperature control accuracy. Flow field non-uniformity degrades the optical performance of liquid lenses. Accurate characterization of physical parameters, including temperature distribution and velocity profiles within fluid flow, is essential for optimizing the thermal and optical performance of immersion techniques.

Numerous flow visualization and measurement techniques have been employed to investigate flow velocity and thermal distribution. These techniques are categorised into intrusive and non-intrusive methods. Intrusive methods, such as thermocouples [4], Pitot tubes and hot-wire anemometry, require inserting sensors directly into the flow to provide data. In contrast, non-intrusive methods, such as Particle image velocimetry (PIV), shadowgraph [5], Schlieren [6, 7], interferometry [8], background-oriented Schlieren (BOS) [9, 10] and laser-induced fluorescent (LIF) [11], enable measurement of velocity and temperature fields without disrupting the flow. However, the aforementioned methods often require separate experimental setups or strict calibration processes for simultaneous temperature and velocity measurements, making them costly and complex to implement in the experiment.

The BOS method represents an innovative adaptation of the traditional Schlieren technique. Dalziel, Carr, Sveen and Davies [9] demonstrated its ability to determine not only the density stratification but also its impact on velocity distribution through the combined use of BOS and PIV techniques. Ihle, Dalziel and Niño [10] advanced the method by introducing a colour separation approach, allowing for simultaneous sampling of multiple parameters. Tokgoz, Geisler, Bokhoven and Wieneke [12] placed a reflective mirror to achieve a single-sided transparent thin fluid layer measurement, combining BOS and PIV to achieve a temperature resolution of less than 1 K. More recently, Vinnicheko [13] combined experimental measurements with numerical solutions of governing equations, using measured BOS data to reconstruct the instantaneous flow parameters in natural convection flows. Similarly, Cai, Wang, Fuest, Jeon, Gray and Karniadakis [14] proposed a

physics-informed neural network (PINN) approach, utilizing tomographic BOS results as input to reconstruct the velocity and pressure fields of the flow over an espresso cup by minimizing a loss function. These hybrid methods, which seamlessly integrate experimental measurements with numerical simulations, are commonly referred to as data assimilation techniques.

According to previous studies, measuring multi-physics flow parameters requires separate experimental setups. And data assimilation reconstruction is typically performed for laminar or natural convection flows, where the temperature field is inherently coupled with the velocity distribution. Therefore, a cost-effective experimental method is required to accurately measure complex temperature distribution and reliably reconstruct the corresponding velocity field. In this study, we proposed a data assimilation technique to reconstruct the velocity field based on the temperature profile obtained using the BOS method, avoiding the need to solve the full set of Navier-Stokes equations. This approach reduces the computational effort by solving only the continuity and momentum equations, excluding the energy equation. Not only natural convection but also mixed convection cases were selected to validate this method. Simulation results were compared with the BOS-reconstructed temperature field and the derived velocity distribution.

2. Reconstruction Methods for Refractive Index and Temperature

2.1. Principles of BOS

The BOS method is a state-of-the-art technique that can character the refractive index of the flow field [9]. It was independently proposed by Dalziel, Hughes and Sutherland [15], Richard and Raffel [16] at the beginning of 21th century. Similar to the classical Schlieren technique, the BOS method reveals the relationship between the ray deflection angle and the refractive index gradient in the fluid. Compared to traditional Schlieren techniques, BOS offers a simpler optical path setup, enables quantitative measurements, and is unaffected by ambient light interference. The schematic diagram of the BOS method is shown in Fig 1. (a) From left to right, including the background pattern, the light source, the schlieren object (flow field), the lens, and the camera. Z_D represents the distance between the centre of the flow field and the background pattern, Z_A is the distance between the centre of the flow field and the lens, Z_B is the distance between the background pattern and the lens, and Z_i is the distance between the lens and the imaging plane.

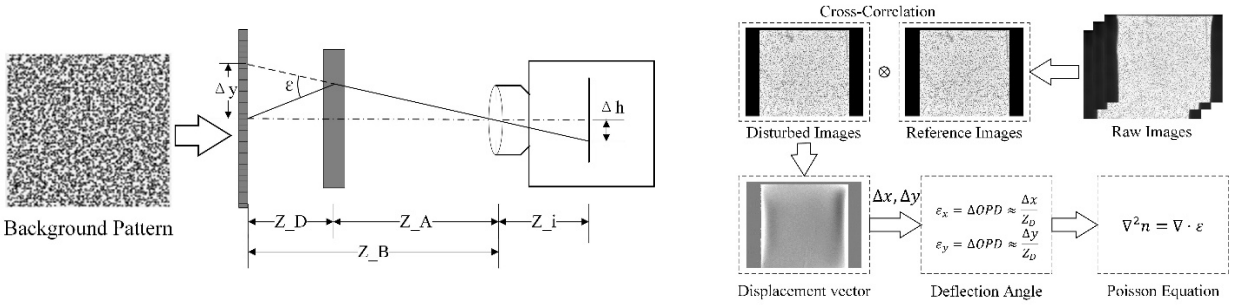

Fig. 1: (a) Schematic of the BOS method; (b) Flow chart of the BOS method.

From the perspective of the camera, under conditions with and without the flow field, the spatial displacement Δy of a background point observed in the field of view corresponds to a displacement Δh on the imaging plane. By applying the paraxial approximation and assuming that the size of the perturbed flow field is negligible compared to its distances from the background and lens, an approximate relationship between the deflection angle ε and the background pattern displacement Δy can be established:

$$\varepsilon \approx \tan \varepsilon = \frac{\Delta y}{Z_D} \tag{1}$$

Since the refractive index of a medium can be expressed as a function of three space coordinates $n = n(x, y, z)$. The passing ray in the phase object is affected with respect to its optical phase and keeps the intensity and amplitude of the ray undisturbed. It is described by Fermat's principle: $\delta \int n(x, y, z)\mathrm{ds} = 0$, where s denote the arc length along the ray. The relationship between the deflection angle ε and the refractive index gradient can be expressed as:

$$\varepsilon \approx \tan\varepsilon = \int \frac{1}{n}\frac{\partial n}{\partial \mathrm{y}}\mathrm{dz} \tag{2}$$

Combining Eq. (1) and (2) the relationship between the displacement Δy and the refractive index gradient is derived. Similarly, the corresponding relationship for the displacement Δx is also obtained.

$$\frac{\partial n}{\partial x} = \frac{\mathrm{n_0}}{\mathrm{W}}\frac{\Delta x}{\mathrm{Z_D}}, \qquad \frac{\partial n}{\partial y} = \frac{\mathrm{n_0}}{\mathrm{W}}\frac{\Delta y}{\mathrm{Z_D}} \tag{3}$$

Where W is the thickness of the test area and $\mathrm{n_0}$ is the nominal refractive index. Assuming the difference between n and $\mathrm{n_0}$ is small. Consider the $\mathrm{n_0}/\mathrm{WZ_D}$ as a constant K, we can apply the divergence operator on both sides of Eq. (3) and construct the Poisson equation:

$$\nabla^2 n = \frac{\partial^2 n}{\partial \mathrm{x}^2} + \frac{\partial^2 n}{\partial \mathrm{y}^2} = \mathrm{K}\left[\frac{\partial}{\partial \mathrm{x}}\Delta x + \frac{\partial}{\partial \mathrm{y}}\Delta y\right] \tag{4}$$

This Poisson equation takes the form $\mathrm{A} \cdot \mathrm{n}(x, y) = \mathrm{g(x, y)}$ with the sparse matrix A, which can be discretized and solved in MATLAB using the mldivide function. Fig 1. (b) has shown the mean procedures of the BOS method.

2.2. Relationship Between Fluid Temperature and Refractive Index

The dependence of the refractive index of water was describe by the well-known Lorenz-Lorenz function. Schiebener, Straub, Levelt Sengers and Gallagher [17] has provided the formulation of the refractive index of water and steam as a function of temperature, density, and the wavelength range from 0.2 to 2.5 μm, temperature range from -12 to 500 ℃ and density range from 0 to 1045 $\mathrm{kg/m^3}$, see Eq. (5). The coefficients of the Eq. (5) are listed in Table 1.

$$\begin{gathered} LL = \frac{\mathrm{n}^2 - 1}{\mathrm{n}^2 + 2}\left(\frac{1}{\rho^*}\right) = \mathrm{a_0} + \mathrm{a_1}\rho^* + \mathrm{a_2}\mathrm{T}^* + \mathrm{a_3}\lambda^{*2}\mathrm{T}^* + \frac{\mathrm{a_4}}{\lambda^{*2}} + \frac{a_5}{\lambda^{*2} - \lambda_{UV}^{*2}} + \frac{a_6}{\lambda^{*2} - \lambda_{IR}^{*2}} + a_7\rho^{*2}, \\ \rho^* = \frac{\rho}{\rho_0}, \rho_0 = 1000\mathrm{kg/m^3}, \qquad \lambda^* = \frac{\lambda}{\lambda_0}, \lambda_0 = 0.589\mu m, \qquad T^* = \frac{T}{T_0}, T_0 = 273.15K. \end{gathered} \tag{5}$$

Table 1: Refractive index formula coefficients of water and water vapor [17].

$\mathrm{a_0} = 0.24425773$	$\mathrm{a_3} = 2.68678472 \times 10^{-4}$	$\mathrm{a_6} = 0.900704920$	$\lambda_{IR} = 5.432937\ \mu m$
$\mathrm{a_1} = 9.74634476 \times 10^{-3}$	$\mathrm{a_4} = 1.58920570 \times 10^{-3}$	$\mathrm{a_7} = -1.66626219 \times 10^{-2}$	
$\mathrm{a_2} = -3.7324996 \times 10^{-3}$	$\mathrm{a_5} = 2.45934259 \times 10^{-3}$	$\lambda_{UV} = 0.2292020\ \mu m$	

$$\rho = \ A \ + \ B(T - T_0) + C(T - T_0)^2 + D(T - T_0)^3 + E(T - T_0)^4 + F(T - T_0)^5 \tag{6}$$

Table 2: NIST density formula coefficients [18].

$\mathrm{A} = 998.846$	$C = -8.55675 \times 10^{-3}$	$E = -4.75911 \times 10^{-7}$	$T_0 = 273.15\ K$
$\mathrm{B} = 6.3606 \times 10^{-2}$	$D = 7.12524 \times 10^{-5}$	$F = 1.39828 \times 10^{-9}$	

The density data can be acquired by fitting the NIST data [18] in Eq. (6), the coefficients of the Eq. (6) are listed in the Table 2. Combining the Eqs (6)-(7), the refractive index $n(x,y)$ can be transmitted to temperature $T(x,y)$.

3. Velocity Field reconstruction Based on the N-S Equation

The method of reconstructing the velocity field is based on the assumption of Boussinesq approximation, which is applied to problems where the fluid varies in temperature. For a general 2D flow with heat transfer, it can be described by the 2D N-S equation including the continuous equation and momentum equation together with the energy equation. The Boussinesq approximation neglects the small density difference except for the gravity force term in the y-momentum equation. The govern equations are shown below.

$$\frac{\partial u}{\partial x}+\frac{\partial v}{\partial y}=0\,, \tag{7}$$

$$\rho_0\left(u\frac{\partial u}{\partial x}+v\frac{\partial u}{\partial y}\right)=\mu_0\left(\frac{\partial^2 u}{\partial x^2}+\frac{\partial^2 u}{\partial y^2}\right)-\frac{\partial p}{\partial x}\,, \tag{8}$$

$$\rho_0\left(u\frac{\partial v}{\partial x}+v\frac{\partial v}{\partial y}\right)=\mu_0\left(\frac{\partial^2 v}{\partial x^2}+\frac{\partial^2 v}{\partial y^2}\right)-\frac{\partial p}{\partial y}-\beta\rho_0(T-T_0)\mathbf{g}\,, \tag{9}$$

$$\frac{\partial T}{\partial t}+u\frac{\partial T}{\partial x}+v\frac{\partial T}{\partial y}=\kappa\left(\frac{\partial^2 T}{\partial x^2}+\frac{\partial^2 T}{\partial y^2}\right). \tag{10}$$

Where $\mathbf{g}$ is the gravity vector, μ_0 and ρ_0 denote the dynamic viscosity and density at temperature T_0, β is the volume coefficient of expansion, and κ refers to the thermal conductivity of the fluid. With the BOS method, Eq. (10) can be omitted, as the temperature field $T(x,y)$ is already obtained and incorporated as the buoyancy force term in Eq. (9), simplifying the problem to the 2D incompressible flow. It is important to note that the boundary conditions are no longer specified, and the flow field essentially behaves as "dead" water without the projection of temperature data. This reconstruction approach involves spatial interpolation between the BOS grid and the CFD computational mesh. The momentum equations are solved with measured temperature and the velocity field can be reconstructed across the flow domain. Using real experiment data can significantly reduce the complexity and cost of the experimental setup while accelerating convergence by omitting the energy equation. To mimic real BOS data, the validation case is fully numerical, given the challenges of obtaining appropriate thermal boundary conditions.

4. Numerical Validation

4.1. Natural Convection Inside a Cubic Enclosure

The first benchmark case is natural convection in a cubic enclosure [19]. Once heating or cooling the vertical boundaries of the liquid chamber, buoyancy force inducing convection circulation develops. This is a semi-2D problem and has plenty of numerical and experimental data to verify. Without loss of generality, the commercial CFD software Ansys Fluent is used to solve the velocity field. The thermal physical properties of the working fluid are presented in Table 3.

Table 3: Thermal physical properties of water, $T_c = 22$℃.

$c_p(J/kg\,K)$	4182.6
$\rho(kg/m^3)$	997.71
$k(W/mK)$	0.60196
$\beta(K^{-1})$	2.15×10^{-4}
$\alpha(m^2/s)$	1.43×10^{-7}
$\mu(Pa\cdot s)$	9.4818×10^{-4}

Fig. 2 (a) depicts the schematic of the square cavity. The horizontal boundaries are assumed to be adiabatic and no-slip, while two vertical boundaries are at constant temperature T_h and T_c. This cavity is filled with water and the Prandtl number is $Pr = 7.02$, and the Rayleigh number is $Ra = 10^6$, the aspect ratio equals 1. The overheat ratio $(T_h - T_c)/T_m = 0.00186$ allows the use of the Boussinesq approximation. Fig. 2 (b) shows the CFD mesh and BOS grid, as a benchmark case, the grid convergence study has been extensively validated [20]. Therefore, an 80×80 nodes grid is chosen. The uniform grid is used in BOS to solve Poisson Eq. (4), while the scaled grid is used in CFD computation. Fig. 2 (c) illustrates the BOS displacement vector field caused by ray deflection due to natural convection.

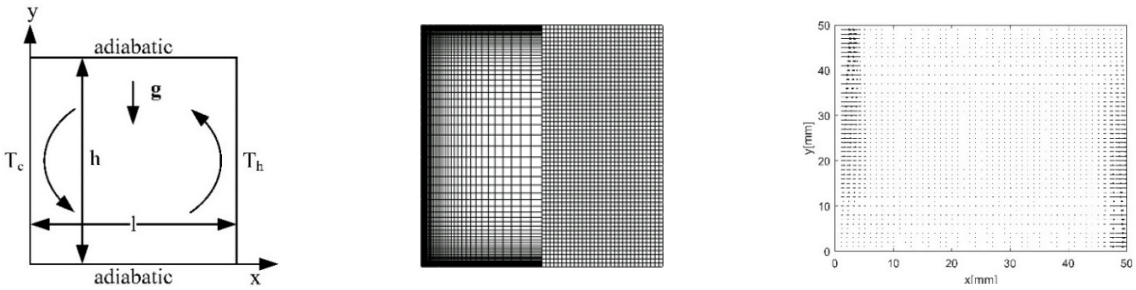

(a) (b) (c)

Fig. 2: (a) natural convection case; (b) Example of meshes (Left: scaled grid; Right: uniform grid); (c) BOS displacement vector

To validate the proposed method, the reference temperature distribution is converted into the refractive index field, and the corresponding BOS displacement vector field is calculated inversely using Eq. (3). A Gaussian filter is applied to smooth the temperature data, and scattered interpolation is used to project CFD results onto the BOS grid. The BOS displacement vector is then implemented in Eq. (4). Following the steps outlined in Sec. 2.2, the solution converged rapidly, given the BOS reconstructed temperature field, as shown in Fig. 3(a). To assess the reconstruction accuracy, the dimensionless temperature $\theta = (T - T_c)/(T_h - T_c)$ along the x-axis was compared with CFD results and experimental reference data [21], as shown in Fig. 3(b). The comparison shows strong agreement, with the reference $\mathrm{Ra} = 4.72 \times 10^6$, while the Ra in both the CFD simulation and reconstruction cases is on the order of 1×10^6, validating the reconstruction method. Then, the reconstruct velocity field is also compared with CFD results and demonstrates great agreements in Figs. (c)-(d). The slightly deviations at the low gradient area of the reconstruction zone could be observed. The maximum difference between the simulated and reconstructed velocity is in the order of 10^5.

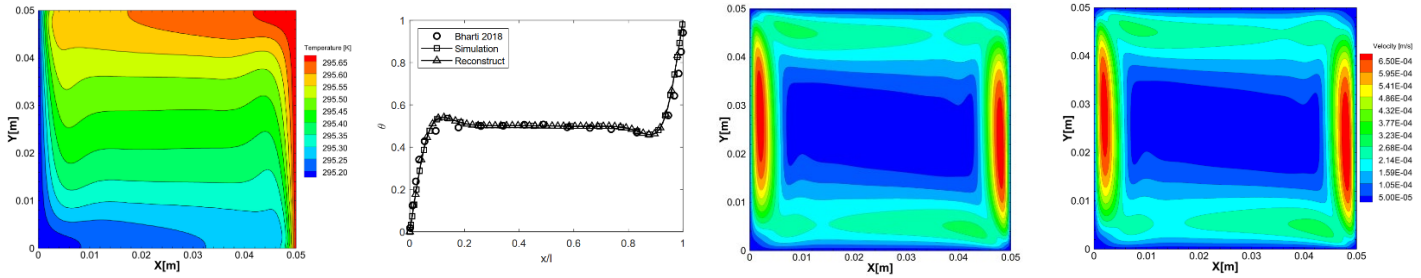

(a) (b) (c) (d)

Fig. 3: (a) BOS reconstruct temperature; (b) Dimensionless comparison; (c) CFD velocity contour; (d) BOS reconstruct velocity

4.2. Mixed Convection Inside a Lid Driven Cavity

The reconstruction of natural convection within a cubic enclosure shows excellent agreement with reference results. The second validation case focuses on mixed convection within a lid-driven cavity. The schematic of this case is similar to the first, except that the top lid is given a constant velocity. The imposed velocity can align with or oppose the direction of the temperature gradient. Other boundary conditions are identical to those in the natural convection case. The primary difference

lies in the top lid velocity, which introduces shear stress that competes with buoyancy forces. Fig. 4 shows the displacement vector distribution for Re = 200, 400 and 800, along with the reversed lid direction case in Re = 200. The streamlines and velocity contours are given in Fig. 5 and 6 respectively. In the mixed convection case, excellent agreement is observed in regions with high temperature gradients, such as near boundary areas. However, discrepancies between the reconstructed and simulated flow become apparent in regions farther away, particularly in low Reynolds number cases. In these cases, buoyancy force is sufficiently strong to compete with the shear stress, and the truncation and numerical errors are surpassed in high temperature gradient region. Conversely, when the buoyancy force is weak, or convection dominates the flow, error terms may prevail, leading to deviations in the results, particularly in the central region of the low Re number cases. The reconstructed flow fields appear to be more diffusive than CFD flow field. The buoyancy force has eliminated two small vortices at the corner of the cubic compare to the traditional lid-driven cavity problem.

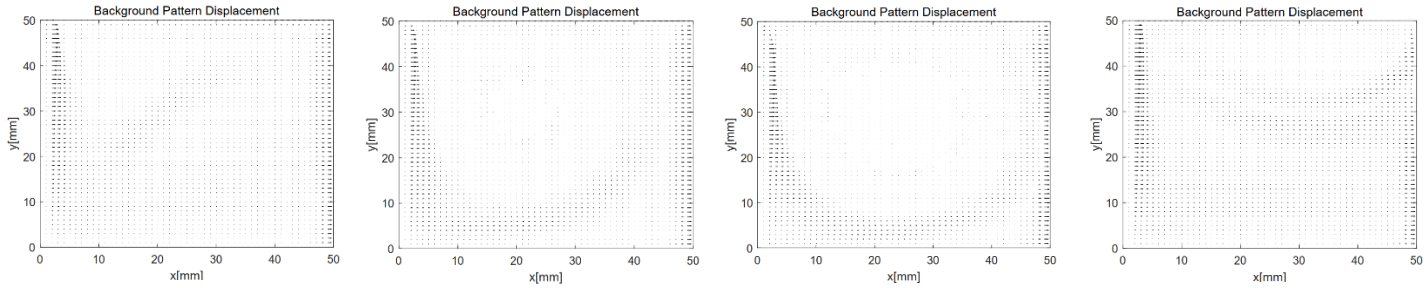

(a) Re = 200 (b) Re = 400 (c) Re = 800 (d) Reversed lid Re = 200

Fig. 4: BOS displacement vector: (a)-(c) u_0 is aligned with temperature gradient, and (d) u_0 is reversed direction.

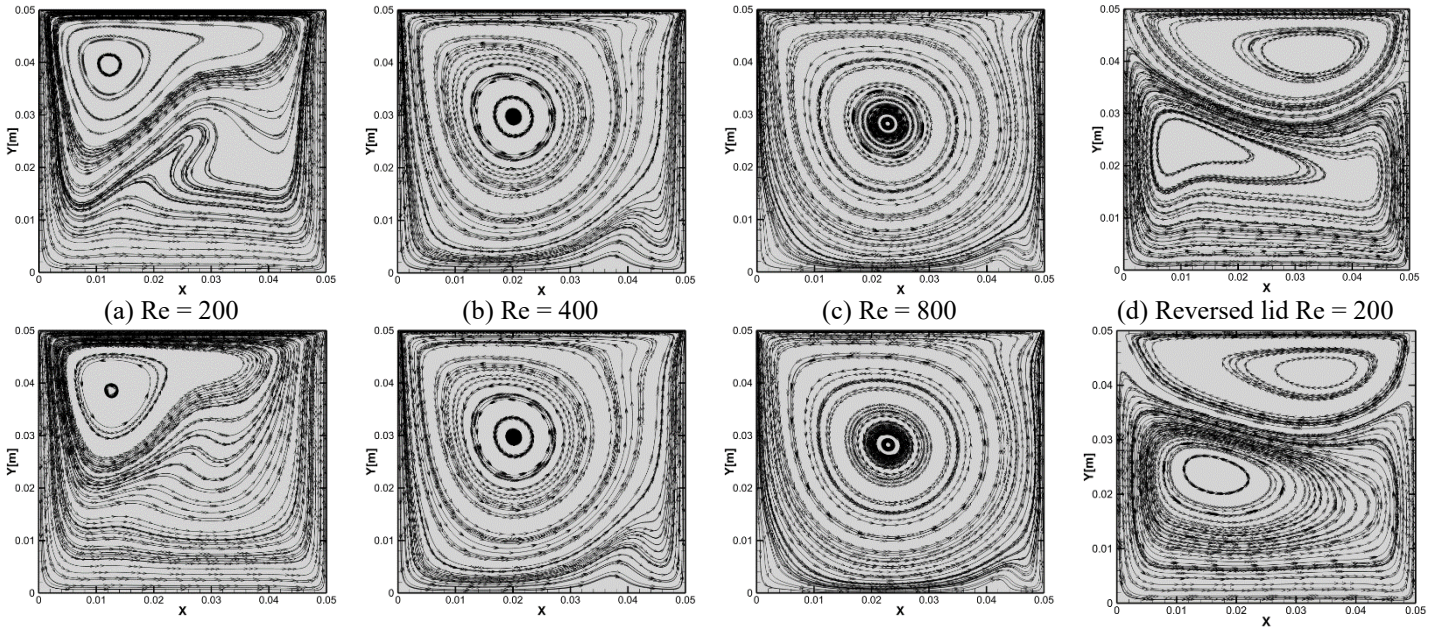

(a) Re = 200 (b) Re = 400 (c) Re = 800 (d) Reversed lid Re = 200

(e) Re = 200 (f) Re = 400 (g) Re = 800 (h) Reversed lid Re = 200

Fig. 5: Streamline comparison: (a)-(d) CFD reference results; (e)-(h) BOS reconstructed flow

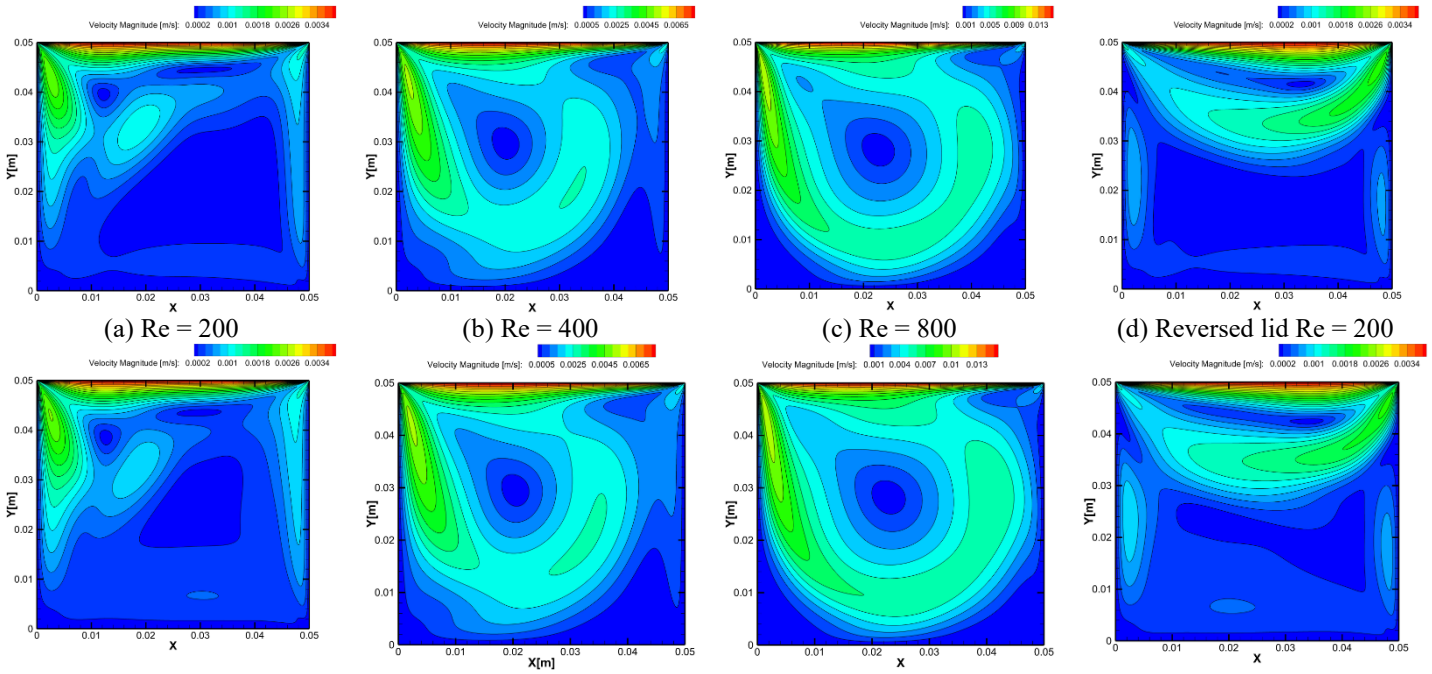

(a) Re = 200 (b) Re = 400 (c) Re = 800 (d) Reversed lid Re = 200

(e) Re = 200 (f) Re = 400 (g) Re = 800 (h) Reversed lid Re = 200

Fig. 6: Velocity contour comparison: (a)-(d) CFD reference results; (e)-(h) BOS reconstructed flow

5. Conclusion

In this study, we proposed a coupled measurement-calculation method to numerically reconstruct the velocity field using BOS-measured temperature in both natural and mixed convection cases. Unlike conventional experimental methods that require separate setups for temperature and velocity measurements, this approach relies solely on the BOS system. The velocity field is numerically derived, providing a cost-effective solution for simultaneously acquiring reliable temperature and velocity field data in fluid flows. This method solves the Navier-Stokes equations without boundary conditions, employs the measured temperature as an initial condition, and excludes the energy equation by incorporating the temperature data in the momentum equation as an additional force term. Quantitative validation was demonstrated with two examples. The accuracy of this approach depends on the following aspects:

1. The BOS resolution relies on experimental setups, including the background pattern, camera capability, placement of optical devices and the resolution of displacement vector fields.

2. Computational errors include discretization and round-off errors, which are introduced during the discretization of partial differential equations in the BOS and CFD processes.

The ability to reconstruct the velocity field using BOS temperature data provides a foundation for assimilating experimental methods with computational approaches to obtain physical data in complex fluid flow. This method can be extended to other flow parameter, such as the density field in a stratified fluid. Since no tracers or markers are introduced into the fluid, it is ideal for ultra-clean environments. Moreover, it is suitable for scenarios involving unknown internal heat sources or complex thermal boundary flow fields.

Acknowledgements

This work was supported by the National Natural Science Foundation of China (This research was supported by the National Natural Science Foundation of China No. 52441504, and Zhejiang Provincial Natural Science Foundation of China under Grant No. LD24E050008).

References

[1] C. Zhang, H. Wang, Y. Huang, L. Zhang, and Y. Chen, "Immersion liquid cooling for electronics: Materials, systems, applications and prospects," *Renew. Sustain. Energy Rev.*, vol. 208, p. 114989, 2025.

[2] Y. Wei and R. L. Brainard, *Advanced Processes for 193-nm Immersion Lithography*. SPIE Press, 2009.

[3] S. Kuiper and B. H. W. Hendriks, "Variable-focus liquid lens for miniature cameras," *Appl. Phys. Lett.*, vol. 85, no. 7, pp. 1128–1130, 2004.

[4] M. S. Bohn, A. T. Kirkpatrick, and D. A. Olson, "Experimental Study of Three-Dimensional Natural Convection High-Rayleigh Number," *J. Heat Transf.*, vol. 106, no. 2, pp. 339–345, 1984.

[5] A. Naghib, J. C. Patterson, C. Lei, and T. Hattori, "Natural convection induced by radiation in a water filled square cavity: Experimental observations," *Exp. Therm. Fluid Sci.*, vol. 80, pp. 105–116, 2017.

[6] A. Martínez-González, J. A. Guerrero-Viramontes, and D. Moreno-Hernández, "Temperature and velocity measurement fields of fluids using a schlieren system," *Appl. Opt.*, vol. 51, no. 16, p. 3519, 2012.

[7] A. Martínez-González, D. Moreno-Hernández, and J. A. Guerrero-Viramontes, "Measurement of temperature and velocity fields in a convective fluid flow in air using schlieren images," *Appl. Opt.*, vol. 52, no. 22, p. 5562, 2013.

[8] J. F. Torres, Y. Zhao, S. Xu, Z. Li, and A. Komiya, "Optical Method for Simultaneous High-Resolution Measurement of Heat and Fluid Flow: The Case of Rayleigh-Benard Convection," *Phys. Rev. Appl.*, vol. 14, no. 5, p. 054038, 2020.

[9] S. B. Dalziel, M. Carr, J. K. Sveen, and P. A. Davies, "Simultaneous synthetic schlieren and PIV measurements for internal solitary waves," *Meas. Sci. Technol.*, vol. 18, no. 3, pp. 533–547, 2007.

[10] C. F. Ihle, S. B. Dalziel, and Y. Niño, "Simultaneous particle image velocimetry and synthetic schlieren measurements of an erupting thermal plume," *Meas. Sci. Technol.*, vol. 20, no. 12, p. 125402, 2009.

[11] S. Eck, M. S. Kharicha, A. Ishmurzin, and A. Ludwig, "Measurement and simulation of temperature and velocity fields during the cooling of water in a die casting model," *Mater. Sci. Eng. A*, vol. 413–414, pp. 79–84, 2005.

[12] S. Tokgoz, R. Geisler, L. J. A. van Bokhoven, and B. Wieneke, "Temperature and velocity measurements in a fluid layer using background-oriented schlieren and PIV methods," *Meas. Sci. Technol.*, vol. 23, no. 11, p. 115302, 2012.

[13] N. A. Vinnichenko, "Obtaining velocity and pressure distributions in natural convection flows using experimental temperature fields," *Appl. Therm. Eng.*, vol. 215, p. 118962, 2022.

[14] S. Cai, Z. Wang, F. Fuest, Y. J. Jeon, C. Gray, and G. E. Karniadakis, "Flow over an espresso cup: inferring 3-D velocity and pressure fields from tomographic background oriented Schlieren via physics-informed neural networks," *J. Fluid Mech.*, vol. 915, p. A102, 2021.

[15] S. B. Dalziel, G. O. Hughes, and B. R. Sutherland, "Whole-field density measurements by 'synthetic schlieren,'" *Exp. Fluids*, vol. 28, no. 4, pp. 322–335, 2000.

[16] H. Richard and M. Raffel, "Principle and applications of the background oriented schlieren (BOS) method," *Meas. Sci. Technol.*, vol. 12, no. 9, pp. 1576–1585, 2001.

[17] P. Schiebener, J. Straub, J. M. H. Levelt Sengers, and J. S. Gallagher, "Refractive index of water and steam as function of wavelength, temperature and density," *J. Phys. Chem. Ref. Data*, vol. 19, no. 3, pp. 677–717, 1990.

[18] N. A. Vinnichenko, A. V. Pushtaev, Y. Yu. Plaksina, Y. K. Rudenko, and A. V. Uvarov, "Horizontal convection driven by nonuniform radiative heating in liquids with different surface behavior," *Int. J. Heat Mass Transf.*, vol. 126, pp. 400–410, 2018.

[19] G. K. Batchelor, "Heat transfer by free convection across a closed cavity between vertical boundaries at different temperatures," *Q. Appl. Math.*, vol. 12, no. 3, pp. 209–233, 1954.

[20] G. Barakos, E. Mitsoulis, and D. Assimacopoulos, "Natural convection flow in a square cavity revisited: Laminar and turbulent models with wall functions," *Int. J. Numer. Methods Fluids*, vol. 18, no. 7, pp. 695–719, 1994.

[21] O. S. Bharti, A. K. Saha, M. K. Das, and S. Bansal, "Simultaneous measurement of velocity and temperature fields during natural convection in a water-filled cubical cavity," *Exp. Therm. Fluid Sci.*, vol. 99, pp. 272–286, 2018.